01 Mar 2020

Understanding Transport of an Elastic, Spherical Particle through a Confining Channel

Shuaijun Li

Honghui Yu

Tai-De Li

Zi Chen

et. al. For a complete list of authors, see https://scholarsmine.mst.edu/civarc_enveng_facwork/1806

Recommended Citation

S. Li et al., "Understanding Transport of an Elastic, Spherical Particle through a Confining Channel," *Applied Physics Letters*, vol. 116, no. 10, American Institute of Physics Inc., Mar 2020.
The definitive version is available at https://doi.org/10.1063/1.5139887

Applied Physics Letters ARTICLE scitation.org/journal/apl

Understanding transport of an elastic, spherical particle through a confining channel

Cite as: Appl. Phys. Lett. **116**, 103705 (2020); doi: 10.1063/1.5139887
Submitted: 22 November 2019 · Accepted: 9 February 2020 ·
Published Online: 11 March 2020

Shuaijun Li,[1] Honghui Yu,[1,a)] Tai-De Li,[2] Zi Chen,[3] Wen Deng,[4,a)] Alimohammad Anbari,[1] and Jing Fan[1,a)]

AFFILIATIONS

[1]Department of Mechanical Engineering, The City College of New York, New York, New York 10031, USA
[2]Advanced Science and Research Center, The City University of New York, New York, New York 10031, USA
[3]Thayer School of Engineering, Dartmouth College, Hanover, New Hampshire 03755, USA
[4]Department of Civil, Architectural and Environmental Engineering, Missouri University of Science and Technology, Rolla, Missouri 65409, USA

[a)]**Authors to whom correspondence should be addressed:** yu@ccny.cuny.edu; wendeng@mst.edu; and jfan1@ccny.cuny.edu

ABSTRACT

The transport of soft particles through narrow channels or pores is ubiquitous in biological systems and industrial processes. On many occasions, the particles deform and temporarily block the channel, inducing a built-up pressure. This pressure buildup often has a profound effect on the behavior of the respective system; yet, it is difficult to be characterized. In this work, we establish a quantitative correlation between the built-up pressure and the material and geometry properties through experiments and mechanics analysis. We fabricate microgels with a controlled diameter and elastic modulus by microfluidics. We then force them to individually pass through a constrictive or straight confining channel and monitor the pressure variation across the channel. To interpret the pressure measurement, we develop an analytical model based on the Neo-Hookean material law to quantify the dependence of the maximum built-up pressure on the radius ratio of the elastic sphere to the channel, the elastic modulus of the sphere, and two constant parameters in the friction constitutive law between the sphere and the channel wall. This model not only agrees very well with the experimental measurement conducted at large microgel deformation but also recovers the classical theory of contact at small deformation. Featuring a balance between accuracy and simplicity, our result could shed light on understanding various biological and engineering processes involving the passage of elastic particles through narrow channels or pores.

Transport of soft particles through narrow channels or pores is ubiquitous in natural and engineering processes. For example, red blood cells squeeze through tiny capillaries;[1,2] tris-acryl gelatin microspheres penetrate into small vessels in therapeutic embolization;[3,4] and preformed particle gels invade into a porous oil reservoir for improved conformance control.[5,6] On many occasions, the soft body deforms and blocks the channel as it moves, inducing a pressure buildup across the channel. This pressure buildup often has a profound effect on the behavior of the biological or industrial system. However, it is challenging, sometimes impossible, to measure this pressure. Instead, we are limited to controlling or measuring the size and material properties of the soft body, the channel size, and the flow properties. Therefore, it is desired to establish a quantitative correlation between the built-up pressure and the measurable or controllable properties. Since many relevant systems involve gel-based soft bodies, several studies have quantitatively investigated the deformation and transport of synthetic hydrogel micro-spheres through tapered or constrictive channels through experimental and analytical methods.[7–12] The experimental studies mostly exclude the friction or adhesion between the microgel and channel wall and focus on the relationship between the pressure, the elastic modulus of microgels, and the geometrical parameters in the equilibrium state.[7–10] To interpret the experimental measurements, analyses were conducted under the assumption of uniform strain and stress distribution.[7–9] Although numerical simulation and mechanics analysis with more general stress–strain relations were attempted, the resulting models are rather complicated and not verified by experiments.[11,12]

In this work, we study the transport of an elastic, spherical particle in a constrictive or straight confining channel with a circular cross section aiming to quantitatively correlate the channel-blockage induced pressure with the radius ratio of the sphere to the channel, the elastic modulus of the particle, and the friction and adhesion properties between the particle and channel wall. We fabricate microgels with

a controlled diameter and properties by microfluidics. We then inject the microgels into circular constrictive or straight confining channels and monitor the built-up pressure. We further develop an analytical model for the built-up pressure based on the Neo-Hookean material law. The model prediction agrees very well with the pressure measurement conducted at large particle deformation, which shows an exponential dependence on the radius ratio. Moreover, the model recovers the classical theory of contact at small deformation. Featuring a balance between simplicity and accuracy, the developed pressure-property correlation could shed light on understanding many industrial and biological processes involving the passage of deformable particles through narrow channels or pores.

We fabricated polyacrylamide microgels with precisely tunable sizes and mechanical properties using microfluidics.[13–15] The constrictive microchannels were made by pulling round glass capillaries with a pipette puller (Sutter Instrument P-1000). The movement of microgels in the channel is driven by a flow rate-controlled syringe pump (Harvard Apparatus PHD 4000). We connected a pressure transducer (Harvard Apparatus P75) to the inlet of the channel to monitor the pressure variation with a temporal resolution of 0.1 s. The channel outlet is open to the atmosphere and at the same horizontal level as the transducer. Here, we adopt the flow rate-controlled method to mimic realistic application scenarios that usually involve non-stop passage of soft particles through confined channels or pores. Therefore, under such a small timescale, the volume change of microgels can be neglected (supplementary material). We observed the movement of microgels under a microscope (Nikon Ts2R) and recorded the process using a digital microscope camera (Nikon DS-Fi2) at a rate of 15 fps. The experimental setup is schematically illustrated in Fig. 1. The fabrication of microgels and constrictive channels is elaborated in the supplementary material.

The motion of a microgel in a constrictive channel can be divided into three stages: (i) before contacting the constriction, (ii) being confined by the constriction, and (iii) after passing the constriction throat. Figure 2(a) displays a microgel at the start and end of stage (ii). At the moment shown in Fig. 2(a-2), the microgel is about to leave the throat, at which point the pressure reaches the maximum. Figure 2(b) plots the variation of pressure and velocity with time as three microgels successively pass the constriction. The flow rate is set to 10 μl/min. Points (a-1) and (a-2) in Fig. 2(b) correspond to Figs. 2(a-1) and 2(a-2), respectively. The pressure starts building up once the microgel comes into contact with and is confined by the channel wall, increases almost

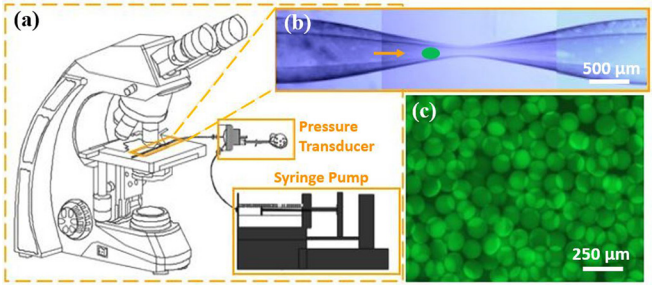

FIG. 1. (a) Schematics of the experimental setup for examining the transport of a microgel in a constrictive channel; (b) micrograph of a constrictive channel; and (c) fluorescence micrograph of microgels.

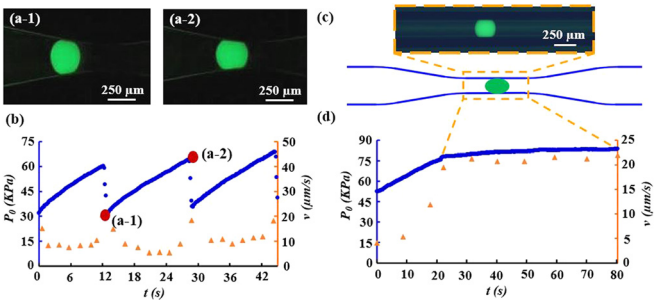

FIG. 2. (a) Fluorescence micrograph of a deformed microgel in a constrictive channel; (b) variation of pressure (P) and microgel velocity (v) with time (t) of three microgels passing the constriction consecutively; (c) fluorescence micrograph of a deformed microgel in a circular straight channel; and (d) variation of pressure (P) and velocity (v) with time (t).

linearly as the microgel moves until reaching the throat, point (a-2), and suddenly drops when the microgel passes the throat. From the velocity profile shown in Fig. 2(b), the velocity of the microgel is approximately constant for the most part, indicating a rough balance between the pressure driving force and the resistance.

Since many biological processes involve the passage of soft bodies in narrow, straight channels, we also injected microgels through a circular straight channel. The fabrication of glass constrictive channels with a narrow straight part in the middle is described in the supplementary material. Figure 2(c) shows a fluorescence micrograph of one deformed microgel moving in the channel. Figure 2(d) shows typical pressure and velocity variation with time. We started recording the pressure when the microgel is confined in the constrictive part, shortly prior to entering the straight section. The flow rate was 10 μl/min before the microgel enters the straight section. Once the microgel enters the straight section, the flow rate is set to 0.2 μl/min to maintain a constant speed for the microgel. According to the Poiseuille law, the pressure drop in the channel due to viscous flow is less than 10 Pa at such a low flow rate. Therefore, the measured pressure is almost exclusively due to channel blockage by microgels. During this process, the pressure remains stable, which balances the constant resistance from the straight channel wall.

We measured and compared the maximum pressure in straight and constrictive channels as a function of the radius ratio Φ of the microgel to the channel. For constrictive channels, the maximum pressure is the pressure at point (a-2) in Fig. 2. We injected microgels into straight channels and constrictive channels with different diameters ranging from 102 μm to 175 μm. The diameter of the microgels is 200 $\pm$ 10 μm. We measured the diameter of each microgel before it enters the narrow or constrictive part and calculated the radius ratio Φ for each gel. The variation of pass-through pressure (maximum pressure) P_0 as a function of Φ is plotted in Fig. 3(a). At the same Φ, the pressure in the constrictive channels is slightly smaller than, but very close to, that in the straight channels. The smaller pressure in constrictive channels is because the entrance and exit angle near the throat results in less confinement as the microgel moves in the throat. In the special case when the channel has a rectangular cross section, a single particle may block the channel and not be able to pass the constriction due to fluid flow in the four corners, whereas multiple particles might pass the constriction cooperatively. Readers may refer to Ref. 16 for a detailed discussion about this phenomenon.

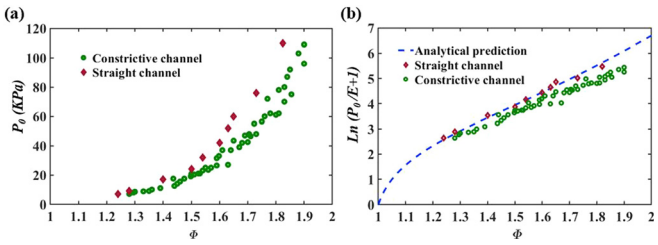

FIG. 3. (a) Pressure variation with radius ratio Φ in constrictive channels (red diamonds) and straight channels (green circles); (b) comparison between analytical prediction and experimental data.

Since the pressure for a microgel passing a constrictive channel with a small entrance angle is similar to that in a straight channel, as shown in Fig. 3(a), for the sake of simplicity without losing accuracy, we analyze a deformed microgel in a straight channel. Figure 4(a) illustrates an originally spherical body with a radius R_0 being confined and deformed in a circular straight channel. The deformed gel experiences a higher hydraulic pressure on its left than right side. We adopt two cylindrical coordinate systems to describe the undeformed and deformed configurations for the convenience of building a governing equation and evaluating integrals. Since the problem is axisymmetric, we use material coordinates *R-Z* for the undeformed reference configuration and Euler coordinates *r-z* for the current deformed body.

The sphere elongates in the *z* axis and contracts in the radial and circumferential directions. We take the ambient environment as the reference state and assume that the pressure at the right side is zero. At the left side, pressure P_0 is applied to drive the sphere, which is moving at a constant velocity along the channel. Consider a gel disk of infinitesimal thickness in the deformed state, as shown in Fig. 4(b). Around the circular edge, the disk is under normal traction σ_r in the radial direction and shear traction τ_w in the axial direction. For simplicity, we assume that the axial normal stress σ_z is uniform in each cross section. We neglect the fluid flow through the permeable microgels

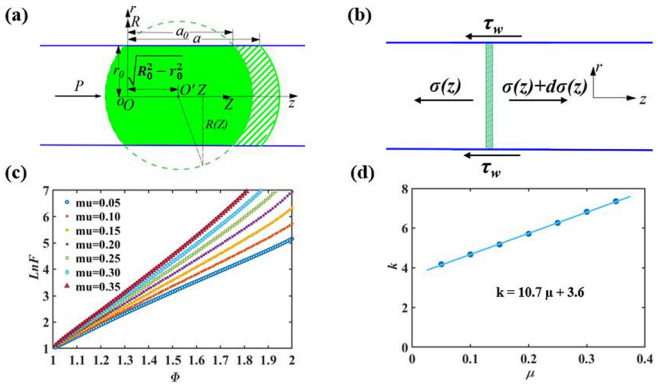

FIG. 4. (a) Illustration of a sphere deformation in a circular straight channel with pressure *P* exerted at the left side. The sphere is assumed to squeeze to the downstream side, and therefore, no deformation occurs at the left side of the sphere. *z* and *Z* axes are along the centerline of the channel toward the direction of the movement. The intersection circle between the undeformed sphere and the channel wall is placed on the $z = 0$ plane; (b) axial normal stress and shear stress on a disk element in the deformed state; (c) variation of *LnF* with Φ and μ; (d) fitting *k*-μ relation.

because the microgel becomes strongly confined in the constriction very quickly in our experiments, as indicated by the rapid increase in the built-up pressure to ~10 kPa within 0.1 s (Fig. 2). At this condition, the microgel is strongly compressed biaxially, resulting in a significant decrease in the pore size of the gel network.[9] We also assume that the hydrodynamic pressure uniformly exerts on the upstream side of the microgel. Therefore, force balance in the axial direction gives

$$\pi r_0^2 d\sigma_z = 2\pi r_0 \tau_w dz, \tag{1}$$

where r_0 is the radius of the channel. We adopt a linear frictional constitutive law to relate τ_w to the normal stress σ_r,[17]

$$\tau_w = \tau_0 - \mu\sigma_r, \tag{2}$$

where τ_0 is a constant parameter, which may be due to surface interaction between the gel and the wall, i.e., adhesion,[18] and μ is a constant parameter that correlates the shear traction τ_w with the normal stress. Combining Eqs. (1) and (2), we have the following differential equation for σ_z:

$$\frac{d\sigma_z}{dz} = \frac{2(\tau_0 - \mu\sigma_r)}{r_0}. \tag{3}$$

For hyperelastic material undergoing large deformation, we need a non-linear stress–strain relation. Considering the material and the range of stretch ratios involved in our experiments, we adopt the Neo-Hookean law for impressible material,[19] which gives

$$\sigma_r - \sigma_z = 2C\left(\lambda_r^2 - \lambda_z^2\right), \tag{4}$$

where $C = E/6$ for incompressible materials and *E* is the modulus of elasticity. λ_r and λ_z are the stretch ratios in the radial and longitudinal direction, respectively. Here, we neglect the gel deswelling that may arise in confined condition since the volume change of the microgels in our experiment is less than 10% for the flow rates we used in the experiments, as shown in the supplementary material. If volume deswelling is significant, we will need to modify the stretch ratios accordingly and consider the property change of the microgels due to deswelling, i.e., the elastic modulus will increase as the volume decreases. For the circular disk in Fig. 4(b) under uniform radial stress around its edge, for the two in-plane normal stress components, $\sigma_r = \sigma_\theta$ and for the two stretch ratios, $\lambda_r = \lambda_\theta$. From incompressibility assumption, $\lambda_r\lambda_\theta\lambda_z = 1$, and consequently, $\lambda_z = 1/\lambda_r^2$. Substituting Eq. (4) into Eq. (3), we obtain a governing differential equation for axial normal stress σ_z,

$$\frac{d\sigma_z}{dz} + \frac{2\mu}{r_0}\sigma_z = \frac{2}{r_0}\left[\tau_0 - \frac{\mu E}{3}\left(\lambda_r^2 - \frac{1}{\lambda_r^4}\right)\right]. \tag{5}$$

This is a first-order ordinary differential equation about σ_z in which λ_r, as a function of *z*, can be independently derived from the radius change. The two spherical caps next to the contact area [Fig. 4(a)] are assumed to be in a hydrostatic state, and hence, $\sigma_z(0) = -P_0$ and $\sigma_z(a) = 0$, with *a* being the length of the contact area. σ_z can be solved by introducing an integrating factor $e^{\int \frac{2\mu}{r_0} dz}$ and fitting the boundary conditions,

$$\sigma_z(a) = e^{-\frac{2\mu}{r_0}z}\left[\int_0^z \left[\frac{2\tau_0}{r_0} - \frac{2\mu E}{3r_0}\left(\lambda_r^2 - \frac{1}{\lambda_r^4}\right)\right] e^{\frac{2\mu}{r_0}z} dz - P_0\right], \tag{6a}$$

where

$$P_0 = \int_0^a \left[\frac{2\tau_0}{r_0} + \frac{2\mu E}{3r_0}\left(\frac{1}{\lambda_r^4} - \lambda_r^2\right)\right] e^{\frac{2\mu}{r_0}z} dz. \quad (6b)$$

Note that $dz = \lambda_z dZ = 1/\lambda_r^2 dZ$, $a = \int_0^{a_0} \lambda_z dZ = \int_0^{a_0} 1/\lambda_r^2 dZ$, $a_0 = 2\sqrt{R_0^2 - r_0^2}$, $\lambda_r = r_0/R(Z)$, and $R(Z) = \sqrt{R_0^2 - \left(Z - \frac{a_0}{2}\right)^2}$. Using the nondimensional parameters $\Phi = R_0/r_0$, $\overline{\tau} = \frac{\tau_0}{E}$, and $\varsigma = Z/a_0$, we have

$$\frac{P_0}{E} = \mu(\Phi^2 - 1)^{1.5} \int_0^1 \frac{16}{3}(\varsigma - \varsigma^2)\left[\left(\Phi^2 - (2\varsigma - 1)^2(\Phi^2 - 1)\right)^2 + \left(\Phi^2 - (2\varsigma - 1)^2(\Phi^2 - 1)\right) + 1\right] e^{4\mu\sqrt{\Phi^2-1}\left[\Phi^2\varsigma - \frac{\Phi^2-1}{6}[(2\varsigma-1)^3+1]\right]} d\varsigma + \frac{\overline{\tau}}{\mu}\left[e^{\frac{4\mu}{3}\sqrt{\Phi^2-1}(2\Phi^2+1)} - 1\right]. \quad (7)$$

Detailed derivation from Eq. (6b) to Eq. (7) is given in the supplementary material. We evaluate the integral in the above equation numerically. Denoting the integral as F, the plot of LnF vs Φ with μ varying from 0.05 to 0.35 is shown in Fig. 4(c). The figure shows that LnF varies with Φ almost linearly. The dependence of the slope k on μ can be fitted as $k = 10.7\,\mu + 3.6$ [Fig. 4(d)]. All the LnF vs Φ lines pass the point (1, 1) independent of the value of μ. Therefore, F can be approximated as $F \cong e^{(10.7\,\mu+3.6)(\Phi-1)+1}$, and Eq. (7) is simplified as

$$\frac{P_0}{E} = \mu(\Phi^2 - 1)^{1.5} e^{(10.7\mu+3.6)(\Phi-1)+1} + \frac{\overline{\tau}}{\mu}\left[e^{\frac{4\mu}{3}\sqrt{\Phi^2-1}(2\Phi^2+1)} - 1\right]. \quad (8)$$

Fitting the experimental data in straight channels (diamonds in Fig. 3) with least squares regression, shown as the blue dashed curve in Fig. 3(b), we find the constant μ to be 0.17 and the nondimensional parameter $\overline{\tau}$ to be 1.6. We measured the modulus of elasticity of microgels using AFM nano-indentation, which has the average value of 0.5 KPa. The details of AFM measurements can be found in the supplementary material. The resultant τ_0 and μ are consistent with previous studies on mechanical properties of gels.[20,21] With only two fitting parameters, Eq. (8) almost exactly captures the dependence of pressure on the radius ratio. The first part of the driving pressure is proportional to E, indicating that it is from the elastic deformation. The second part of the pressure is proportional to the adhesion constant τ_0, related to the radial compression through μ, but independent of E.

When Φ is close to unity, the sphere and channel have a small contact and Eq. (8) has a simple asymptotic expression, $\frac{P_0}{E} = \mu\left(\sqrt{\Phi^2 - 1}\right)^3 e + 4\overline{\tau}\sqrt{\Phi^2 - 1}$, in which $\sqrt{\Phi^2 - 1}$ represents the half contact length normalized by the radius of the channel, with the higher order terms being ignored. Consequently, the first term in the asymptotic expression indicates that the normal contact force is proportional to the third power of the contact length, which is consistent with classical Hertz theory of contact,[22] and the second term, the contribution from the adhesion, is proportional to the contact length. Different from the large contact, now, the adhesion and radial compression are decoupled. Eq. (8) not only gives the exponential dependence of driving pressure on radius ratio Φ at a large scale contact but also recovers the classical asymptotic behavior at a small contact.

In this work, we studied the deformation and passage of an elastic sphere in narrow constrictive or straight channels through both experiments and mechanics analysis. We found how the maximum built-up pressure in a blocked channel (pass-through pressure) varies with the radius ratio of the sphere to channel, the elastic modulus of the sphere, and two constant parameters in the friction constitutive law between the sphere and channel wall. We fabricated microgels with a well-controlled size and properties using microfluidics and monitored the pressure variation when the microgels were forced through a straight or constrictive channel one at a time. At the same radius ratio, the pass-through pressures for constrictive and straight channels are almost the same given that the entrance angle of the constriction is small. To gain quantitative understanding of the pass-through pressure, we establish a differential equation for the axial normal stress by balancing axial forces on an infinitesimal deformed disk element in the circular channel. The Neo-Hookean material law is adopted for elastic deformation, which is applicable to a variety of elastomers, including highly stretchable hydrogels. We then find the relation among the driving pressure, material properties, and geometrical parameters by solving the differential equation. This analytical model, featuring sufficient simplicity and rooting from rigorous analysis, predicts the measured pass-through pressure as spherical microgels move in constrictive channels at large deformation. Moreover, the model recovers the classical theory of contact at small deformation. We expect that the model can be used to interpret a variety of biological and engineering processes involving the passage of elastic particles through narrow channels. For pressure-controlled systems, if the particle is stuck in the channel and thus deswelling, we can also use the model to estimate how much the gel should shrink before passing through the channel. In order to accurately capture this process, a rate-dependent model is currently being developed. The methodology of developing this model can be readily extended to some non-spherical particles as well, such as ellipsoid and circular cylinders. We are currently working on deriving a universal model for several particle geometries, which involves some parameters that characterize the geometry. We expect that the pressure would have a similar dependence on the radius mismatch of the particle to the constriction.

See the supplementary material for more details on the microfluidic fabrication of microgels, the fabrication of constrictive and straight channels, the evaluation of gel deswelling, the measurement of elastic modulus of the microgels, and the analytical derivation of Eq. (7).

J.F. acknowledges the support from The City College of New York and American Chemical Society Petroleum Research Fund (No. 57496-DNI9).

REFERENCES

[1]J. L. McWhirter, H. Noguchi, and G. Gompper, Soft Matter **7**, 10967 (2011).
[2]R. Skalak and P. I. Branemark, Science **164**, 717 (1969).
[3]M. Bendszus, R. Klein, R. Burger, M. Warmuth-Metz, E. Hofmann, and L. Solymosi, AJNR Am. J. Neuroradiol. **21**, 255 (2000).
[4]J. B. Spies, C. Cornell, R. Worthington-Kirsch, J. C. Lipman, and J. F. Benenati, J. Vasc. Interventional Radiol. **18**, 203 (2007).
[5]B. J. Bai, L. X. Li, Y. Z. Liu, H. Liu, Z. G. Wang, and C. M. You, SPE Reservoir Eval. Eng. **10**, 415 (2007).
[6]B. J. Bai, Y. Z. Liu, J. P. Coste, and L. X. Li, SPE Reservoir Eval. Eng. **10**, 176 (2007).
[7]H. M. Wyss, T. Franke, E. Mele, and D. A. Weitz, Soft Matter **6**, 4550 (2010).
[8]Y. Li, E. Kumacheva, and A. Ramachandran, Soft Matter **9**, 10391 (2013).

[9]Y. Li, O. S. Sariyer, A. Ramachandran, S. Panyukov, M. Rubinstein, and E. Kumacheva, Sci. Rep. **5**, 17017 (2015).
[10]S. Hu, R. Wang, C. M. Tsang, S. W. Tsao, D. Sun, and R. H. W. Lam, RSC Adv. **8**, 1030 (2018).
[11]W. H. Lei, C. Y. Xie, T. J. Wu, X. C. Wu, and M. R. Wang, Sci. Rep. **9**, 1453 (2019).
[12]C. Giverso, A. Grillo, and L. Preziosi, Biomech. Model. Mechanobiol. **13**, 481 (2014).
[13]G. M. Whitesides, Nature **442**, 368 (2006).
[14]P. Gravesen, J. Branebjerg, and O. S. Jensen, J. Micromech. Microeng. **3**, 168 (1993).
[15]R. Seemann, M. Brinkmann, T. Pfohl, and S. Herminghaus, Rep. Prog. Phys. **75**, 016601 (2012).
[16]M. G. O'Connell, N. B. Lu, C. A. Browne, and S. S. Datta, Soft Matter **15**, 3620 (2019).
[17]J. R. Rice, N. Lapusta, and K. Ranjith, J. Mech. Phys. Solids **49**, 1865 (2001).
[18]J. Yang, R. Bai, B. Chen, and Z. Suo, Adv. Funct. Mater. **30**, 1901693 (2019).
[19]M. C. Boyce and E. M. Arruda, Rubber Chem. Technol. **73**, 504 (2000).
[20]S. Schmidt, M. Zeiser, T. Hellweg, C. Duschl, A. Fery, and H. Möhwald, Adv. Funct. Mater. **20**, 3235 (2010).
[21]J. Gong, Y. Iwasaki, and Y. Osada, J. Phys. Chem. B **103**, 6001 (1999).
[22]K. L. Johnson, *Contact Mechanics* (Cambridge University Press, 1985).